IDENTIFICATION OF MATERIAL PARAMETERS OF SILICONE WITH HYPERELASTIC MATERIAL MODELS BY FEM

THANH-TUNG NGUYEN ^{1,2}, SY-TUAN HOANG³, THI-MINH-KIEU TRAN¹

¹Department of Textiles - Footwear and Fashion, School of Material Science and Engineering, Hanoi University of Science and Technology, Vietnam

²Faculty of Garment Technology and Fashion Design, Hanoi University of Industry, Vietnam

³Department of Mechatronics, School of Mechanical Engineering, Hanoi University of Science and Technology, Vietnam

DOI: 10.17973/MMSJ.2025_11_2025091

corresponding author: tuan.hoangsy@hust.edu.vn

The purpose of this study is to determine the material parameters of platinum-cured silicone using uniaxial tensile testing combined with hyperelastic material models to simulate material deformation via the finite element method (FEM). Experimental data from uniaxial tensile tests were used to estimate and capture the material behavior based on selected hyperelastic models. Matlab software was employed to fit experimental data and calculate material parameters, which were subsequently implemented in FEM simulations using Ansys Workbench. Simulation results were compared experimental data. The findings indicate that the Mooney-Rivlin model provides the best agreement with the experimental results. Initial numerical simulations, assuming ideal incompressibility, produced reasonable approximations but failed to fully reproduce actual behavior. Therefore, material compressibility must be considered. By introducing nearincompressibility coefficients corresponding to Poisson's ratios, it was found that a value of 0.41 yielded very high consistency between experimental and simulated results. Modeling the nonlinear elastic deformation of hyperelastic materials is critical for both material development and product design. This study highlights the importance of incorporating compressibility in modeling, thereby improving accuracy and practical applicability. The outcomes provide a foundation for employing platinum-cured silicone simulations in the design and fabrication of external breast prostheses for post-mastectomy patients.

KEYWORDS

Nonlinear FEM, Hyperelastic materials, Numerical modelling, Platinum-cured silicone

1 INTRODUCTION

Silicone materials have been widely applied in modern life due to their outstanding mechanical properties. They are utilized across various industries including aerospace, defense, automotive, construction, electronics, healthcare, and food processing sectors [Han et al. 2022; Shit et al. 2013]. Silicone is also employed in the fabrication of human body prostheses [Al Kadah et al. 2018; Gaikwad et al. 2019; Weisson et al. 2020], including external breast prostheses for women who have

undergone mastectomy as part of breast cancer treatment [Zeng et al. 2021; Leme et al. 2023; Cancercouncil 2023].

Similar to rubber and other elastomers, silicone exhibits nearincompressibility and isotropy [Steinmann et al. 2012], as well as a high elongation capacity under relatively small loads [Hamdi et al. 2006]. In the small-strain region (low stress), the material can be approximated using linear elastic models with corresponding Young's modulus and shear modulus. Under large deformations, silicone exhibits hyperelastic behavior—nonlinear rubber-like elasticity—where stress increases nonlinearly with stretch and the material can recover its original shape upon unloading. Common hyperelastic material models used to simulate silicone include: Neo-Hookean (single-parameter), Mooney-Rivlin (typically two-parameter or extended to 3-5 parameters), Yeoh (based on strain invariants such as the first invariant I₁, second I₂, or third I₃), and Ogden (using exponential forms of first-, second-, or third-order) [Marckmann et al. 2006; Kim et al. 2012; Cârlescu et al. 2012; Carlescu et al. 2014; Marckmann et al. 2017]. The parameters of these hyperelastic models can be identified from experimental data, such as uniaxial tension [Lavazza et al. 2023; Marl et al. 2024; Nandasiri et al. 2020; Mollaee et al. 2024], biaxial tension [Arm et al. 2024; Jobst et al. 2022], uniaxial compression [Gao et al. 2024; Zulkifli et al. 2023], or volumetric deformation tests [Li et al. 2025]. These models are suitable for describing the nonlinear elastic behavior of rubber-like materials with isotropic and nearly incompressible properties. Several recent studies have compared these models to determine the most suitable one for simulating silicone. Results show that the third-order Yeoh model performs well for moderate deformation ranges, while the second- or third-order Ogden model is more appropriate for very large deformations [Phothiphatcha et al. 2021]. However, some studies also indicate that the five-parameter Mooney-Rivlin model provides good agreement with experimental data for silicone [Gao et al. 2024; Zulkifli et al. 2023]. Silicone typically has a low elastic modulus, in the range of a few hundred kilopascals, and a low Shore A hardness [Miranda, 2021; Baban, 2024]. Its Poisson's ratio is approximately 0.5 due to its near-incompressibility, making it similar to biological soft tissues [Miranda et al. 2021]. Platinumcured silicone is non-toxic, heat-resistant, and soft. In the event of rupture or perforation, it is not absorbed by the skin, thus ensuring high biocompatibility [Johnshopkinsmedicine 2025]. Silicone can be molded to resemble the natural shape of a breast or partial breast depending on the type of surgery (e.g., partial or total unilateral mastectomy). Therefore, it is commonly used in breast augmentation for aesthetic purposes or as an external prosthetic breast to replicate the natural contour following mastectomy [Cancercouncil 2023; Eggbeer et al. 2011].

In this study, silicone material will be modeled using the finite element method (FEM) to describe its large, nonlinear deformation behavior based on experimental data. This will enable the determination of material parameters, serving as a basis for simulation and design of breast prosthesis.

2 THEORETICAL BASIS

For rubber-like hyperelastic material models, the right and left Cauchy-Green deformation tensors, respectively **C** and **B**, are defined by [Bonet et al. 1997; Holzapfel 2000]:

$$\mathbf{C} = \mathbf{F}^T \mathbf{F}, \qquad \mathbf{B} = \mathbf{F} \mathbf{F}^T \tag{1}$$

where $\boldsymbol{\mathsf{F}}$ is deformation gradient.

The three same principal invariants I_1 , I_2 và I_3 of ${\bf C}$ and ${\bf B}$ are given by

$$I_1 = \operatorname{tr}(\mathbf{C}) \tag{2}$$

$$I_2 = \frac{1}{2} [(\text{tr}\mathbf{C})^2 - \text{tr}(\mathbf{C}^2)]$$
 (3)

$$I_3 = \det \mathbf{C} \tag{4}$$

Stretch ratios are defined as the square roots of the eigenvalues of $\bf C$ and is denoted as (λ_i) i=1;2;3. Then the three same principal invariants are also determined based on the eigenvalues of $\bf C$:

$$I_1 = \lambda_1^2 + \lambda_2^2 + \lambda_3^2 \tag{5}$$

$$I_2 = \lambda_1^2 \lambda_2^2 + \lambda_2^2 \lambda_3^2 + \lambda_3^2 \lambda_1^2$$
 (6)

$$I_3 = \lambda_1^2 \lambda_2^2 \lambda_3^2 \tag{7}$$

The relationship between the stress tensor $\boldsymbol{\sigma}$ and the nominal stress tensor \boldsymbol{P} is determined by the formula:

$$\mathbf{P} = \det(\mathbf{F}\mathbf{\sigma}\mathbf{F}^{-T}) \tag{8}$$

The strain energy function is calculated according to

$$W = W(\mathbf{C}) = \psi(\lambda_1, \lambda_2, \lambda_3) \tag{9}$$

The stress tensor is determined as below equation

$$\sigma_i = J^{-1} \lambda_i \frac{\partial \psi}{\partial \lambda_i} \qquad i = 1, 2, 3 \tag{10}$$

where J is the volume ratio, given by:

$$J = \lambda_1 \lambda_2 \lambda_3 \tag{11}$$

In the case of an ideal incompressible solid, the volume ratio J=1, principal invariant $I_3=\det {\bf C}=\det {\bf B}=\lambda_1^2\lambda_2^2\lambda_3^2=J^2=1$.

For nearly incompressible hyperelastic materials, the strain energy function is used by:

$$W = W_{iso}(\mathbf{F}) - p(J-1) \tag{12}$$

where $J = \det \mathbf{F} = \lambda_1 \lambda_2 \lambda_3 = 1$.

The nominal stress **P** is determined by:

$$\mathbf{P} = \frac{\partial W_{iso}}{\partial \mathbf{F}} - p\mathbf{F}^{-T} \tag{13}$$

The stress tensor is determined by equation:

$$\mathbf{\sigma} = -p\mathbf{I} + \mathbf{F} \frac{\partial W_{iso}}{\partial \mathbf{F}} \tag{14}$$

In the case of an uniaxial tension test, $\lambda_2=\lambda_3=\lambda_1^{-1/2}$, with $\lambda_1=\lambda$, then $\sigma_1=\sigma$, $\sigma_2=\sigma_3=0$. The stress tensor is calculated by:

$$\sigma = 2\left(\lambda^2 - \frac{1}{\lambda}\right) \left(\frac{\partial W_{iso}}{\partial I_1} + \frac{1}{\lambda} \frac{\partial W_{iso}}{\partial I_2}\right) \tag{15}$$

3 EXPERIMENTAL

3.1 Specimen Preparation

Three dog-bone experimental samples were created by two component silicone gel, mixing ratio of 50/50. The parameters of silicone announced by the manufacturer are shown in Tab. 1.

Table 1. Silicone material properties

Material	Density (g/cm3)	Tensile Strength (MPa)	Tear Strength (kN/m)	Viscosity (mPa.s)	у
Platinum- cured silicone	1.13	6.0 ± 1.0	23 ± 5	6000 1500	±

Silicone was poured into the mold and degassed under vacuum to remove air bubbles, forming a thin film of 2 mm thickness. After completely curing the membrane, it will be cut in a dogbone shape according to DIN 53504-S3A standards with the dimensions shown in Fig. 1.

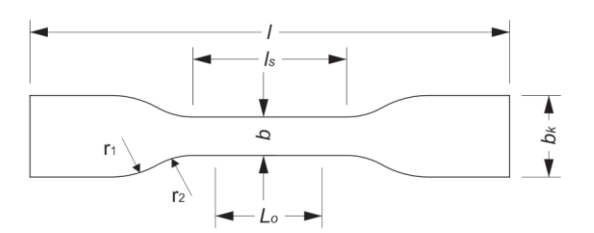


Figure 1 : Dimensions of test samples according to DIN 53504-S3A (1994)

Where:

I - minimum overall length: 50mm *b*_k - width of ends: 8.5 ± 0.5mm I_s - length of narrow parallel portion: 16 ± 1mm b - width of narrow parallel portion: 4 ± 0.1mm r_1 - large radius: 10 ± 0.5mm r_2 - small radius: 7.5 ± 0.5mm L₀ - initial gauge length: 10_{mm} a – thickness 2 ± 0.2mm

The dog-bone-shaped specimens were fabricated by casting liquid silicone rubber into aluminum molds and subsequently cured at room temperature for 24 hours. After demolding, the samples were conditioned at ambient temperature (23 \pm 2 °C) and relative humidity (50 \pm 5%) for at least 48 hours prior to testing to ensure thermal and mechanical equilibrium.

3.2 Experimental Setup

The tensile tests performed using Lloyd Instruments LS1 universal testing machine (AMETEK, UK) equipped with a 100 N load cell and pneumatic grips to prevent slippage, Fig. 2. The crosshead displacement was measured with an internal encoder, and load was recorded simultaneously through the machine's data acquisition system. The gauge length and specimen dimensions were measured with a precision digital caliper before each test



Figure 2: Tensile test

to ensure compliance with the DIN 53504–S3A standard.

Each specimen was mounted carefully between the grips to ensure alignment along the loading axis. The tests were carried out under uniaxial tension at a constant crosshead speed of 200 mm/min, as recommended by the standard for elastomeric materials. The force–displacement data were continuously recorded until specimen rupture.

3.3 Hyperelastic Material Modelling

The nominal stress was calculated by dividing the measured force by the initial cross-sectional area of the specimen. The nominal strain was determined from the ratio of the crosshead displacement to the initial gauge length. For hyperelastic material characterization, the true stress and true strain were further derived using the incompressibility assumption. The experimental data were subsequently used to fit hyperelastic constitutive models (Mooney–Rivlin, Neo-Hookean, Ogden) through nonlinear regression using MATLAB.

These models are suitable for the characteristics of silicone and ease of modeling [Zulkifli et al. 2023]. Furthermore, previous studies on rubber-like material modeling have been conducted

using these hyperelastic models [Marckmann et al. 2017; Zulkifli et al. 2023; Ali et al. 2010; Thanakhun et al. 2019].

The strain energy function based on the Mooney-Rivlin 2-parameter model is chosen by [Mooney 1940; Rivlin 1948a]:

$$W_{iso} = C_{10}(I_1 - 3) + C_{01}(I_2 - 3)$$
 (16)

From (15), then the stress tensor is determined by equation.:

$$\sigma = 2\left(C_{10} + \frac{C_{01}}{\lambda_1}\right) \left(\lambda_1^2 - \frac{1}{\lambda_1}\right) \tag{17}$$

where C_{10} and C_{01} are Mooney–Rivlin 2-parameter material parameters.

The strain energy function based on the Mooney-Rivlin 5-parameter model is chosen by [Mooney 1940; Rivlin 1948a]:

$$W_{iso} = C_{10}(I_1 - 3) + C_{01}(I_2 - 3) + C_{11}(I_1 - 3)(I_2 - 3) + C_{20}(I_1 - 3)^2 + C_{02}(I_2 - 3)^2$$
(18)

where C_{10} , C_{01} , C_{20} , C_{11} and C_{02} are Mooney–Rivlin material parameters

From (15), then the stress tensor is determined by equation:

$$\sigma = 2 \begin{bmatrix} C_{10} + C_{11}(I_2 - 3) + C_{20}(I_1 - 3) \\ + \frac{C_{01} + C_{11}(I_1 - 3) + C_{02}(I_2 - 3)}{\lambda_1} \end{bmatrix} \left(\lambda_1^2 - \frac{1}{\lambda_1} \right)$$
 (19)

The strain energy function based on the Neo–Hookean model is chosen by [Rivlin 1948b] :

$$W_{iso} = C_{NH}(I_1 - 3) (20)$$

where C_{NH} is neo–Hookean material parameter.

From (15), then the stress tensor is determined by equation:

$$\sigma = 2C_{NH} \left(\lambda_1^2 - \frac{1}{\lambda_1} \right) \tag{21}$$

The strain energy function based on the Ogden model is chosen by [Ogden 1972]:

$$W_{iso} = \sum_{n=1}^{1} \frac{\mu_n}{\alpha_n} \left(\lambda_1^{\alpha_n} + \lambda_2^{\alpha_n} + \lambda_3^{\alpha_n} - 3 \right)$$
 (22)

where μ_n and α_n are material constants for Ogden model, and n represents the number of Ogden terms used.

Therefore, from (15) the stress tensor is determined by equation:

$$\sigma = \sum_{n=1}^{N} \mu_n (\lambda_1^{\alpha_n} - \lambda_1^{-\alpha_n/2})$$
 (23)

where (μ_n, α_n) n = 1, N are the material parameters that satisfy the condition

$$\mu_n \alpha_n > 0 \quad \forall \ n = 1, N \tag{24}$$

Material parameters of different hyperelastic models such as Mooney-Rivlin, Ogden or Neo-Hookean are estimated using Matlab software. The data of the uniaxial tensile test is the basis for determining material parameters. Material parameters determined by Matlab software are used for numerical simulation of materials using Ansys Workbench software.

4 RESULTS AND DISCUSSION

4.1 Material parameters

Tab. 2 lists the material parameter values corresponding to the hyperelastic material models, estimated in MATLAB using the least-squares method.

Table 2: Values of material parameters corresponding to hyperelastic models

No	Models	Parameters
1	2-Parameter Mooney-Rivlin	$C_{01} = -0.13937 \text{ MPa}$; $C_{10} = 0.15014 \text{ MPa}$
2	5-Parameter Mooney Rivlin	$C_{10} = 0.15223 \text{ MPa}$; $C_{01} = -0.13646 \text{ MPa}$; $C_{20} = 0.073424 \text{ MPa}$ $C_{11} = -0.14949 \text{ MPa}$; $C_{02} = 0.045751 \text{ MPa}$
3	Neo-Hookean	C _{NH} = 0.090097 MPa
4	One-term Ogden	$\mu_1 = 0.021437 \text{ MPa}$; $\alpha_1 = 5.0043$

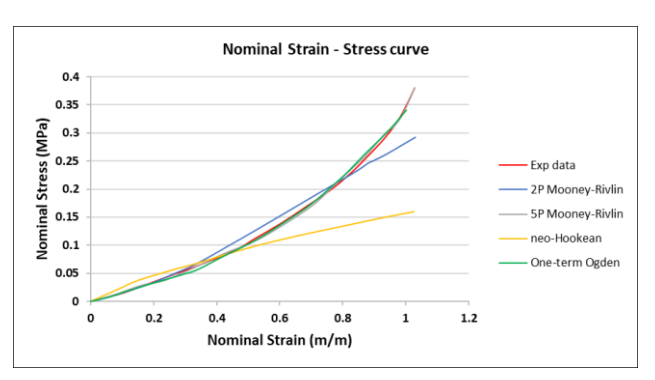
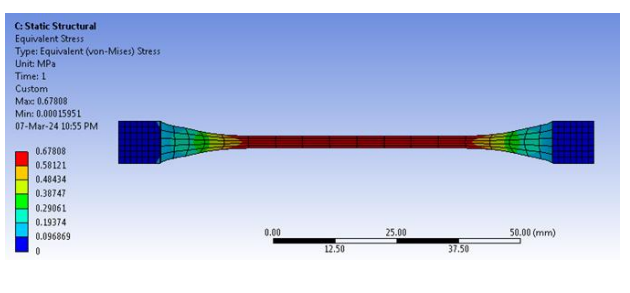


Figure 3: Stress—strain curves estimated from hyperelastic models.

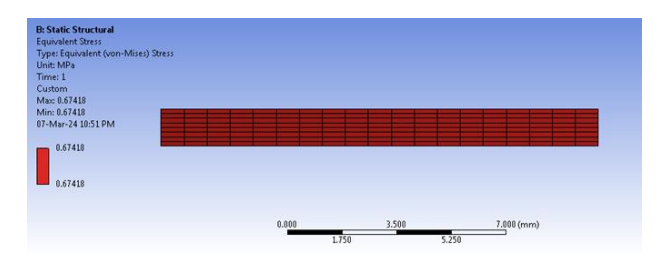
Simulation plots in Fig. 3 show that the stress–strain curves from the 5-parameter Mooney–Rivlin and Ogden models closely match the experimental data. The 2-parameter Mooney-Rivlin model shows a slight deviation. In contrast, the curves for the Neo-Hookean model deviate noticeably from the experimental data points.

4.2 Numerical simulation results in FEM

FEM simulations with Mooney-Rivlin, Ogden or Neo-Hookean hyperelastic models are calculated with models built-in Ansys Workbench. The 3D model of the sample was built with dimensional parameters as shown in Fig. 1. The boundary conditions applied in the FEM model are set at both ends of the test sample, with one fixed end and one moving end, corresponding to the sample areas in real are fastened between the clamping of the tensile device [Sasso et al. 2008].



(a)



(b)

Figure 4: FEM simulation of uniaxial tension sample: (a) full model, (b) quarter model

Initial simulation results on Ansys as shown in Fig. 4-a show that the test length has uniform stress and strain in the deformation observing area. Therefore, to simplify the numerical simulation results, we have built one-eighth of the test sample with dimensions of 5x2x1mm, the results are shown in Fig. 4-b.

The stress and strain simulation data of hyperelastic models with incompressibility assumption (D=0) are extracted and compared with experimental results, as shown in Fig. 5.

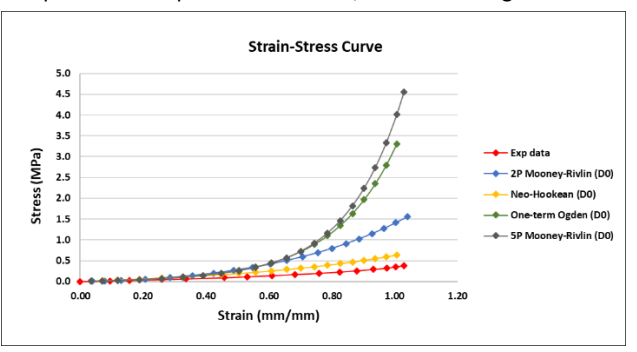


Figure 5 : Stress–strain curves for incompressible assumption (D = 0)

Fig. 5 depicts that there is a difference in the Stress - Strain curve between the numerical simulation results and the experimental results. This may be due to the fact that some compressibility of the material still exists, meaning that D is non-zero. To evaluate this possibility, numerical simulations with different values of Poisson's coefficient ν close to 0.5 are implemented in order to determine the parameter D.

Then, the strain energy function used by:

$$W = W_{iso} + \frac{1}{D}(J - 1)^2$$
 (25)

where J is the determinant of the elastic deformation gradient \mathbf{F} and D is the material incompressibility parameter, is determined by equation:

$$D = \frac{2}{K} \tag{26}$$

where K is Bulk modulus, is defined by:

$$K = \frac{2G(1+v)}{3(1-2v)} \tag{27}$$

where G is Shear modulus, is defined by:

$$G = \frac{\partial^2 W}{\partial \gamma^2} \bigg|_{\gamma=0} \tag{28}$$

where γ is simple shear.

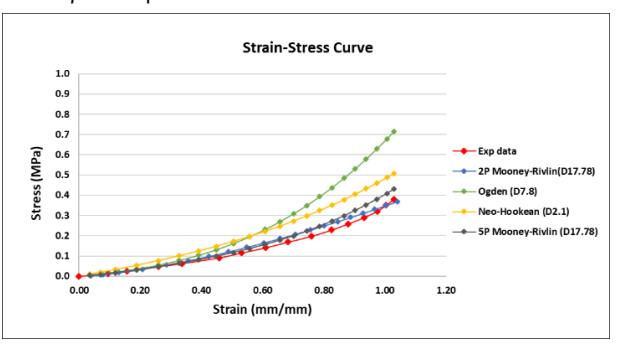


Figure 6: Stress-strain curves for compressible models with varying D

The results in Fig. 6 show that, with Poisson's coefficient by 0.41, the Stress - Strain curves of experimental and numerical results for the hyperelastic models has approximately the same forms. This shows that the initial statement that D is non-zero has scientific basis. As Poisson's coefficient $\nu=0.41$, the incompressibility coefficients D of the material corresponding to the hyperelastic models are determined. The results are listed in Tab. 3.

Table 3 : Compressible hyperelastic model parameters ($\nu = 0.41$)

No.	Models	Parameters
1	2-parameter Mooney-Rivlin	$C_{01} = -0.13937 \text{ Mpa}$; $C_{10} = 0.15014 \text{ MPa}$; $D = 17.78 \text{ MPa-1}$
2	5-parameter Mooney-Rivlin	$C_{10} = 0.15223 \; \text{MPa}$; $C_{01} = -0.13646 \; \text{MPa}$; $C_{20} = 0.073424 \; \text{MPa}$; $C_{11} = -0.14949 \; \text{MPa}$ $C_{02} = 0.045751 \; \text{MPa}$; $D = 17.78 \; \text{MPa-1}$
3	Neo-Hookean	$C_{NH} = 0.090097 \text{ MPa}$; $D = 2.1 \text{ MPa-1}$
4	Ogden	μ_1 = 0.021437 MPa ; α_1 = 5.0043 ; D = 7.8 MPa-1

5 CONCLUSION

Rubber-like materials can be modeled by nonlinear elastic theory based on conventional hyperelastic material models such as the Mooney-Rivlin, Ogden or Neo-Hookean models. The classification of the models is presented based on the range of values for all deformation types, the number of parameters and the type of formula are used to derive the model. Therefore, it depends on the deformation domain considered; The Neo-Hookean model, Mooney-Rivlin model and Ogden model can be used appropriately for small, medium and large deformations, respectively.

Uniaxial tensile test is commonly applied to reveal the mechanical properties of hyperelastic materials and then their data is used to calculate material parameters. The first numerical simulation results were applied to ideal incompressible material models, giving reasonable approximate results but unable to accurately reproduce the material behavior. Therefore, the compressibility of the material must be taken into account in material models. Following the experimental data, the hyperelastic material models were investigated with different material nearly incompressibility coefficient values. The results

denoted that the incompressibility material coefficient corresponds to Poisson's ratio ν = 0.41, showing very high agreement between experimental results and numerical simulation results. These results can serve as reliable input parameters for further numerical simulations.

REFERENCES

- [Al Kadah et al. 2018] AL KADAH, B., NAUMANN, A., SCHNEIDER, M., SCHICK, B., LINXWEILER, M. & PAPASPYROU, G. 2018. Auricular reconstruction with polyethylene implants or silicone prosthesis: A single institution experience. *Journal of Cranio-Maxillofacial Surgery*, 46, 2150-2156. https://doi.org/10.1016/j.jcms.2018.10.005.
- [Ali et al. 2010] ALI, A., HOSSEINI, M. & SAHARI, B. 2010. A review and comparison on some rubber elasticity models.

 Journal of Scientific & Industrial Research, 69, 495-500.
- [Arm et al. 2024] ARM, R., SHAHIDI, A., PISLARU, A., MARASINGHE, K., BIBB, R. & HUGHES-RILEY, T. 2024.

 Mechanical Behavior of Oil-Saturated Silicone Membranes for Adipose Tissue Synthesis in Clinical and Theatrical Prosthesis. *Prosthesis*, 6, 1340-1358. https://doi.org/10.3390/prosthesis6060097
- [Baban, 2024]BABAN, N. Biotrojans: viscoelastic microvalve-based attacks in flow-based microfluidic biochips and their countermeasures. Sci. Rep. 14 (2024). https://doi.org/10.1038/s41598-024-70703-0
- [Bonet et al. 1997] BONET, J. & WOOD, R. D. 1997. Nonlinear continuum mechanics for finite element analysis, Cambridge university press.
- [Cancercouncil 2023] CANCERCOUNCIL. 2023. Breast prostheses and reconstruction [Online]. Available: https://www.cancercouncil.com.au/cancerinformation/managing-cancer-side-effects/breast-prostheses-and-reconstruction/breast-prostheses/material-used/ [Accessed 2025].
- [Cârlescu et al. 2012] CÂRLESCU, V., OLARU, D., PRISĂCARU, G. & VLAD, S. 2012. Determining the stress-strain curve of PDMS-SiO2-TiO2 electroactive polymers. Mechanical Testing and Diagnosis, 2, 54-61.
- [Carlescu et al. 2014] CARLESCU, V., PRISACARU, G. & OLARU, D. 2014. FEM simulation on uniaxial tension of hyperelastic elastomers. *Applied Mechanics and Materials*, 659, 57-62. https://doi.org/10.4028/www.scientific.net/AMM.659.57
- [Eggbeer et al. 2011] EGGBEER, D. & EVANS, P. 2011. Computeraided methods in bespoke breast prosthesis design and fabrication. Proceedings of the Institution of Mechanical Engineers, Part H: Journal of Engineering in Medicine, 225, 94-99. https://doi.org/10.1243/09544119JEIM755
- [Gaikwad et al. 2019] GAIKWAD, A. M., RAM, S. M., NADGERE, J. B. & SHAH, N. P. 2019. Recreating first digit with silicone prosthesis. *National Journal of Maxillofacial Surgery*, 10, 105-108. https://doi.org/10.4103/njms.NJMS 59 18
- [Marckmann et al. 2017] MARCKMANN, G. & VERRON, E. 2017. Efficiency of hyperelastic models for rubber-like

- [Gao et al. 2024] GAO, J., XU, Z., HAN, R., QI, Z. & HAN, G. 2024.

 Refinement of hyperelastic models based on tension and compression experiments of polydimethylsiloxane (PDMS). *Mechanics of Solids*, 59, 955-965. https://doi.org/10.1134/S0025654424602659
- [Hamdi et al. 2006] HAMDI, A., ABDELAZIZ, M. N., AÏT HOCINE, N., HEUILLET, P. & BENSEDDIQ, N. 2006. A fracture criterion of rubber-like materials under plane stress conditions. Polymer Testing, 25, 994-1005. https://doi.org/10.1016/j.polymertesting.2006.06.00 5.
- [Han et al. 2022] HAN, R., LI, Y., ZHU, Q. & NIU, K. 2022. Research on the preparation and thermal stability of silicone rubber composites: A review. *Composites Part C: Open Access*, 8, 100249. https://doi.org/10.1016/j.jcomc.2022.100249
- [Holzapfel 2000] HOLZAPFEL, A. G. 2000. Nonlinear solid mechanics II.
- [Jobst et al. 2022] JOBST, S. & STOMMEL, M. 2022. Experimental and simulative characterization for material and lifetime modelling of a silicone adhesive. *International Journal of Adhesion and Adhesives*, 113, 103042. https://doi.org/10.1016/j.ijadhadh.2021.103042
- [Johnshopkinsmedicine 2025] JOHNSHOPKINSMEDICINE. 2025.

 Post-Mastectomy Prosthesis [Online]. Available:

 https://www.hopkinsmedicine.org/health/treatmenttests-and-therapies/postmastectomy-prosthesis
 [Accessed 2025].
- [Kim et al. 2012] KIM, B., LEE, S. B., LEE, J., CHO, S., PARK, H., YEOM, S. & PARK, S. H. 2012. A comparison among Neo-Hookean model, Mooney-Rivlin model, and Ogden model for chloroprene rubber. *International Journal of Precision Engineering and Manufacturing*, 13, 759-764. https://doi.org/10.1007/s12541-012-0099-y
- [Lavazza et al. 2023] LAVAZZA, J., CONTINO, M. & MARANO, C. 2023. Strain rate, temperature and deformation state effect on Ecoflex 00-50 silicone mechanical behaviour. *Mechanics of Materials*, 178, 104560. https://doi.org/10.1016/j.mechmat.2023.104560.
- [Leme et al. 2023] LEME, J. C., DE OLIVEIRA SPINOSA, R. M., LEAL, S. O., HIRSCH, A. B. B., LODOVICO, A., STRAMANDINOLI-ZANICOTTI, R. T., KUNKEL, M. E. & MOURA, F. A. 2023. Development of low-cost and personalized external silicone breast prosthesis produced by additive manufacturing for women who have undergone mastectomy: A pilot study. *Clinical Biomechanics*, 110, 106123. https://doi.org/10.1016/j.clinbiomech.2023.106123
- [Li et al. 2025] LI, J., XIE, Z., VARNER, H., CHOCKALINGAM, S. & COHEN, T. 2025. Cylindrical cavity expansion for characterizing mechanical properties of soft materials. Extreme Mechanics Letters, 77, 102343. https://doi.org/10.1016/j.eml.2025.102343
- [Marckmann et al. 2006] MARCKMANN, G. & VERRON, E. 2006.

 Comparison of hyperelastic models for rubber-like materials. Rubber chemistry and technology, 79, 835-858. https://hal.science/hal-01004680v1 materials. Constitutive Models for Rubber IV. Routledge. https://hal.science/hal-01004682

- [Marl et al. 2024] MARL, S., NI, X., HORNIG, T., SPIEKER, C., GIESEN, R.-U., HEIM, H.-P. & FISTER, M. 2024. Correlations between the Aging Behavior and Finite Element Method Simulation of Three Silicone Elastomers". Materials 17.16 (2024): 3961. https://doi.org/10.3390/ma17163961
- [Miranda, 2021] MIRANDA, I., SOUZA, A., SOUSA, P., RIBEIRO, J., CASTANHEIRA, E. M., LIMA, R. & MINAS, G. 2021. Properties and applications of PDMS for biomedical engineering: A review. *Journal of functional biomaterials*, 13, 2. https://doi.org/10.3390/jfb13010002
- [Mollaee et al. 2024] MOLLAEE, S., HAJIRASSOULIHA, A., BUDGETT, D. M., TABERNER, A. J. & NIELSEN, P. M. 2024. Model-based design of a pneumatic actuator for a dynamically reconfigurable socket for transtibial amputees. Frontiers in Bioengineering and Biotechnology, 12, 1459056. https://doi.org/10.3389/fbioe.2024.1459056
- [Mooney 1940] MOONEY, M. 1940. A theory of large elastic deformation. *Journal of applied physics*, 11, 582-592.
- [Nandasiri et al. 2020] NANDASIRI, G. K., IANAKIEV, A. & DIAS, T. 2020. Hyperelastic properties of platinum cured silicones and its applications in active compression. *Polymers*, 12, 148. https://doi.org/10.3390/polym12010148
- [Ogden 1972] OGDEN, R. W. 1972. Large deformation isotropic elasticity—on the correlation of theory and experiment for incompressible rubberlike solids. *Proceedings of the Royal Society of London. A. Mathematical and Physical Sciences*, 326, 565-584.
- [Phothiphatcha et al. 2021] PHOTHIPHATCHA, J. & PUTTAPITUKPORN, T. 2021. Determination of material parameters of PDMS material models by MATLAB. Engineering Journal, 25, 11-28. https://doi.org/10.4186/ej.2021.25.4.11
- [Rivlin 1948a] RIVLIN, R. S. 1948a. Large elastic deformations of isotropic materials IV. Further developments of the general theory. *Philosophical transactions of the royal society of London. Series A, Mathematical and physical sciences*, 241, 379-397.
- [Rivlin 1948b] RIVLIN, R. S. 1948b. Large elastic deformations of isotropic materials. II. Some uniqueness theorems for pure, homogeneous deformation. *Philosophical*

- Transactions of the Royal Society of London. Series A, Mathematical and Physical Sciences, 240, 491-508.
- [Sasso et al. 2008] SASSO, M., PALMIERI, G., CHIAPPINI, G. & AMODIO, D. 2008. Characterization of hyperelastic rubber-like materials by biaxial and uniaxial stretching tests based on optical methods. *Polymer Testing*, 27, 995-1004.
 - https://doi.org/10.1016/j.polymertesting.2008.09.00
- [Shit et al. 2013] SHIT, S. C. & SHAH, P. 2013. A review on silicone rubber. *National academy science letters*, 36, 355-365. https://doi.org/10.1007/s40009-013-0150-2
- [Steinmann et al. 2012] STEINMANN, P., HOSSAIN, M. & POSSART, G. 2012. Hyperelastic models for rubber-like materials: consistent tangent operators and suitability for Treloar's data. *Archive of Applied Mechanics*, 82, 1183-1217. https://doi.org/10.1007/s00419-012-0610-z
- [Thanakhun et al. 2019] THANAKHUN, K. & PUTTAPITUKPORN, T. 2019. PDMS material models for anti-fouling surfaces using finite element method. *Engineering Journal*, 23, 381-398. https://doi.org/10.4186/ej.2019.23.6.381
- [Weisson et al. 2020] WEISSON, E. H., FITTIPALDI, M., CONCEPCION, C. A., PELAEZ, D., GRACE, L. & TSE, D. T. 2020. Automated noncontact facial topography mapping, 3-dimensional printing, and silicone casting of orbital prosthesis. *American journal of ophthalmology*, 220, 27-36. https://doi.org/10.1016/j.ajo.2020.06.032
- [Zeng et al. 2021] ZENG, L., XIE, X.-Q., LUO, T., ZHANG, H., KANG, J.-B., WANG, F. & LI, X.-F. 2021. Progress of radiotherapy after breast-conserving surgery combined with silicone prosthesis reconstruction.

 European Review for Medical & Pharmacological Sciences, 25.

 https://doi.org/10.26355/eurrev 202103 25210
- [Zulkifli et al. 2023] ZULKIFLI, N. A., MOON, G. D., HYUN, D. C. & LEE, S. 2023. Comprehensive constitutive modeling and analysis of multi-elastic polydimethylsiloxane (PDMS) for wearable device simulations. *Scientific reports*, 13, 18413. https://doi.org/10.1038/s41598-023-45372-0

CONTACTS:

Dr. SY-TUAN HOANG
Department of Mechatronics, School of Mechanical
Engineering, Hanoi University of Science and Technology,
Vietnam
tuan.hoangsy@hust.edu.vn